Journal of Materials Chemistry A

Accepted Manuscript

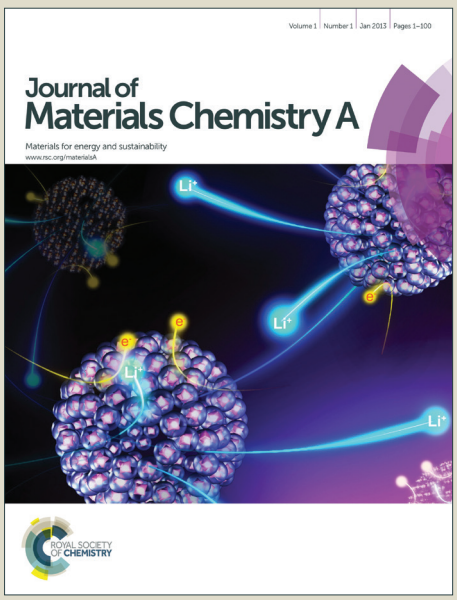

ROYAL SOCIETY OF CHEMISTRY

www.rsc.org/materialsA

Journal Name

RSCPublishing

ARTICLE

Nanodisperse ZIF-8/PDMS Hybrid Membranes for Biobutanol Permselective Pervaporation†

Hongwei Fan, Naixin Wang, Shulan Ji, Hao Yan, Guojun Zhang*

Cite this: DOI: 10.1039/x0xx00000x

Received 00th January 2012,
Accepted 00th January 2012

DOI: 10.1039/x0xx00000x

www.rsc.org/

Alcohol-permselective membranes may have an increasingly important role in bioalcohol production. Developments for this membrane mostly involve hybrid membranes. Obtaining high compatibility and nanodispersion of inorganic nanoparticles in the polymer matrix is the key to fabricating hybrid membranes with high pervaporation performance. In this study, a homogeneous, nanodisperse ZIF-8/PDMS membrane was prepared by repeated immersion of a polysulfone supporting membrane in a dilute ZIF-8/PDMS suspension and subsequent removal of defects using a concentrated PDMS solution. To improve the nanoscale dispersion of ZIF-8, the nascent ZIF-8 suspension was directly dispersed in a PDMS solution without drying. This procedure avoids aggregation and redispersion of ZIF-8 nanoparticles after forming a powder. Analyses confirmed that the ZIF-8–PDMS dispersion effectively diminished aggregation between nanoparticles and led to the formation of a well-dispersed ZIF-8/PDMS membrane. A homogeneous and thin ZIF-8/PDMS permselective layer was obtained by adjusting the preparation conditions. The prepared ZIF-8/PDMS membrane exhibited high separation factor (52.81) and high flux (2800.5 g m^{-2} h^{-1}) in the separation of 5.0 wt.% *n*-butanol/water solution at 80 °C. By comparing the powder-dispersed ZIF-8/PDMS hybrid membrane against the suspension-dispersed ZIF-8/PDMS membrane, we found that latter showed much higher performance in butanol separation. Therefore, the nanodisperse ZIF-8/PDMS membrane has great potential application for in situ recovery of biobutanol.

1. Introduction

Development of renewable and clean biofuels has been a great concern confronted by research into new energy resources.[1–4] Biobutanol, one of the most valuable biofuels, is mainly produced by fermentation from renewable biomass. The final product of butanol in fermentation broths is alcohol-in-water solutions,[5,6] which is typically dilute mainly because of severe product inhibition and toxicity of the product butanol.[7,8] Pervaporation technique is the most promising technology for recovering biobutanol from aqueous solution because it is energy-saving, cost-effective, and harmless to microorganisms compared with conventional distillation and extraction.[9–11] In particular, organophilic pervaporation can be integrated with a bioreactor to achieve continuous fermentation, can effectively enhance conversion rates, and can yield high concentrations of bioalcohols.[12–14]

The core of the organophilic pervaporation process is developing a butanol-selective membrane with high flux and high selectivity. However, recent developments in polymeric membrane materials have apparently reached their limit in separation performance. For example, the reported butanol–water separation factors for the most common polymeric membrane material, polydimethylsiloxane (PDMS), generally range from 15 to 50, and the total fluxes are normally <1.0 kg m^{-2} h^{-1}.[15–23] Thus, the pervaporation performance of these polymer membranes still do not meet the requirements of industrial applications for butanol recovery.[8] Development of inorganic membrane materials are restricted by high fabrication costs[24] and by the lack of maturity of the preparation method,[25,26] although some inorganic membranes are known to perform better than do polymeric membranes.[27,28]

Incorporation of hydrophobic particle fillers such as silicalite, zeolite, silica, carbonaceous frameworks, and metal-organic frameworks (MOFs) (e.g., zeolitic imidazolate frameworks) in the polymer matrix has recently been proven to be a facile and cost-effective way to prepare hybrid membranes and to improve their performance.[29–39] These materials are therefore typically used in studies on alcohol-permselective membranes.[40,41] Obtaining high compatibility and high degree of nanodispersion of inorganic nanoparticles in the polymer matrix is the key to fabricating hybrid membranes with high pervaporation performance in bioalcohol recovery from aqueous solution.[42–44] One significant issue is poor

compatibility of inorganic particle fillers and polymeric phases and serious agglomeration of inorganic nanoparticles in the polymer matrix. This easily leads to defects in the prepared membranes, ultimately resulting in little or no improvement in selectivity over the original polymer membranes.[45–47] Another challenge is the distinct tradeoff relationship between the permeability and selectivity of hybrid membranes.[43,48]

The recently developed MOF–polymer hybrid membranes perform well in separation in the recovery of alcohol from aqueous solution because of the high adsorption selectivity of alcohol and super-hydrophobicity of its MOF materials.[36,38,39,49,50] Moreover, MOF materials are highly compatible with the polymer matrix because of the organic linkers present in the frameworks.[51,52] However, agglomeration of MOF nanoparticles in the polymer cross-linking layer limits further improvement of the alcohol-permselective performance.[51,53] Various approaches have been taken to achieve a high degree of dispersion of MOF hybrid membranes, including prepolymerization of the polymer solution, stirring, and sonication with a probe-type sonicator or ultrasonic bath.[48,54–57] To date, these methods are not effective enough to prevent agglomeration of MOF nanoparticles in membrane-preparation processes.[36,38,39,58,59] This limitation is due to the strong interactions between MOF nanoparticles after the standard drying procedure.[51]

Thus, approaches to effectively overcome or to minimize agglomeration of MOF nanoparticles in membrane formation are necessary to obtain well-dispersed MOF–polymer hybrid membranes. In this study, a nanodisperse ZIF-8/PDMS nanohybrid membrane was prepared by repeated immersion of a polysulfone (PS) supporting membrane in a dilute ZIF-8/PDMS solution followed by removal of defects using a relatively concentrated PDMS solution (post-treatment). To improve the nanoscale dispersion of ZIF-8, the nascent ZIF-8 suspension that had not been dried further was directly dispersed in a PDMS solution. This avoids aggregation and redispersion of ZIF-8 nanoparticles after forming the powder. The synthesized well-dispersed ZIF-8/PDMS nanohybrid membrane was therefore expected to show better performance in biobutanol pervaporation. The effects of preparation condition on the membrane morphologies and pervaporation performance were studied in detail.

2. Experimental

2.1 Materials

Zinc nitrate hexahydrate ($Zn(NO_3)_2 \cdot 6H_2O$) and 2-methylimidazole (Hmim) were purchased from Sigma-Aldrich and were used as received. PDMS with viscosity of 20,000 Pa·s was purchased from China Bulestar Chengrand Chemical Co., Ltd. Tetraethoxysilane (TEOS), *n*-heptane, dibulytin dilaurate (DBTDL), methanol, ethanol, and *n*-butanol were purchased from Beijing Chemical Factory. All chemicals were of analytical grade and were used without further purification. Flat-sheet PS ultrafiltration membranes with a nominal molecular weight cutoff of 20,000 (PS-20) were supplied by Sepro Membranes. Ultrapure water was prepared by using an RU water purification system (RiOs16, Millipore).

2.2 Preparation of ZIF-8 suspension and nanoparticles

ZIF-8 nanocrystals were synthesized at room temperature through a procedure described in a previous report.[60] A solution of $Zn(NO_3)_2 \cdot 6H_2O$ (2.933 g, ≥99.0%) in 200 mL of methanol was rapidly poured into a solution of Hmim (6.489 g, 99%) in 200 mL of methanol under stirring at room temperature. The mixture, which slowly acquired a milky color, was continuously stirred for 1.5 h. The nanocrystals formed were subsequently separated by centrifugation and then washed with fresh ethanol. The nanocrystals were then directly redispersed in a small amount of fresh ethanol without the drying step to form a stable ZIF-8/ethanol suspension for later use. For comparisons, the ZIF-8 powder nanoparticles were also prepared after drying the nanocrystals at 40 °C overnight.

2.3 Membrane preparation

The PS ultrafiltration sheet membranes were used as supports. After pretreatment with 30 wt.% ethanol aqueous solution, the membranes were rinsed with ultrapure water to remove the residual ethanol on the surface and then re-immersed in a filter flask full of ultrapure water. A vacuum pump was used to provide negative pressure for extracting air from the membrane pores over a period of 4 h. Afterward, the PS membranes were allowed to dry at room temperature until no free water on the surface could be observed.

To improve the nanoscale dispersion of ZIF-8 in PDMS solution, quantitative ZIF-8/ethanol suspensions (varied from 17.7 wt.% to 46.3 wt.%) that had not been dried was directly dispersed dropwise in a dilute PDMS/*n*-heptane solution (1 wt.%, 250mL) (Labeled as suspension-dispersed ZIF-8/PDMS). TEOS (1 wt.%) and DBTDL (0.05 wt.%) were then added, and the mixture was stirred for another 0.5 h. The ZIF-8/PDMS mass ratio of ZIF-8/PDMS suspension varied from 0.5:1 to 2:1 . The ZIF-8 content of the suspension based on dry weight of the ZIF-8 powder was known. The effect of ethanol content of the suspension was expected to be negligible because of its very low volume and its miscibility with *n*-heptane. In addition, a concentrated PDMS pre-cross-linked solution (10 wt.%) was prepared. The preparation process for the ZIF-8/PDMS membrane is illustrated in Scheme 1. First, a homogeneous ZIF-8/PDMS membrane was formed by repeatedly and horizontally dipping the pre-treated PS supporting membrane in a ZIF-8/PDMS solution (1 wt.%) (1 min immersion per layer, 30 s intervals). After each dipping, the membranes were taken out and then fixed perpendicularly onto a substrate with a rotating motor. The membranes rotated with the rotating motor at a speed of 100 rpm were continuously baked by a burner. In this case, the residual solution on the support surface could be effectively removed. Thereafter, the as-prepared nascent ZIF-8/PDMS membrane was dipped once in a concentrated PDMS pre-cross-linked solution (10 wt.%, 1 min immersion) to cover potential defects. Afterward, the finished membranes were allowed to stand for 1 day in air at room temperature. Finally, the membranes were placed in a convection oven set at 80 °C for 8 h to fully cross-link the PDMS solution. For comparison, dry ZIF-8 powder nanoparticles were redispersed in PDMS solution with a probe-type sonicator and used for the preparation of ZIF-8/PDMS hybrid membrane through the same procedure (Labeled as powder-dispersed ZIF-8/PDMS). Additionally,

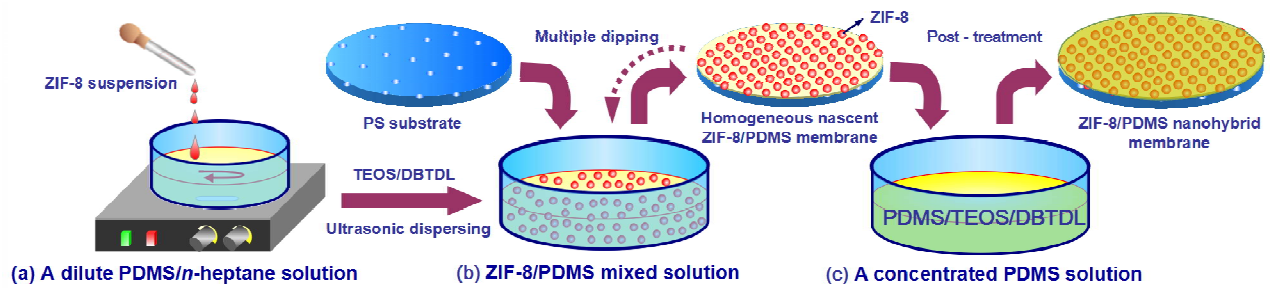

Scheme. 1 Preparation process of the suspension-dispersed ZIF-8/PDMS nanohybrid membrane.

an unfilled PDMS composite membrane was also prepared in the same manner as described above.

2.4 Characterization techniques

Morphologies of the synthesized ZIF-8 nanoparticles were examined by scanning electron microscopy (SEM) and energy-dispersive spectrometry (EDS) (Hitachi S-4300, Japan). Images of the surfaces and cross sections of the membranes were obtained. Cross sections of the membranes were prepared by freeze-fracture after immersion in liquid nitrogen for several minutes. Prior to observations, all samples were coated with gold in vacuum to increase their conductivity.

Dispersion of the ZIF-8 nanoparticles in PDMS solution was examined by transmission electron microscopy (TEM; JEM-2010, JEOL, Ltd., Japan). To prepare the TEM sample, a drop of each of the suspension-dispersed and powder-dispersed ZIF-8/PDMS (1:1, w/w) solutions were applied onto two ultrathin carbon films. The carbon films were dried under vacuum at room temperature overnight before observation.

The size distribution of ZIF-8 particles in the liquid at 25 °C was measured by dynamic light scattering (DLS; Dynapro Titan TC, Wyatt Technology Corporation). All of the samples were stored at room temperature for 24 h before measurement. Size distribution curves for each sample were obtained three times and then averaged.

Hydrophobic properties of the ZIF-8 nanoparticles and membranes were characterized through sessile drop method by measuring static water contact angles of the surfaces with a contact angle meter (DSA100, Krüss, Germany). ZIF-8 nanoparticles were poured onto slides and then compressed into flakes before measurement. The volume of water droplet used in the measurements was 5 μL. *n*-Butanol contact angles of the surfaces were measured in the same way as that for water, the only difference being that the contact angle was recorded until a stable value was reached. Contact angles at five different positions of each sample were measured and then averaged.

X-ray diffraction (XRD) patterns of the membranes and ZIF-8 nanoparticles were obtained on a Bruker D8 Advance diffractometer (Cu K_α X-ray radiation, $\lambda = 1.54$ Å). Each XRD pattern was acquired from 5° to 45° at a rate of 0.02° s^{-1}. All XRD data described here were recorded at 40 kV voltage and 40 mA current applied to the X-ray rotating anode.

2.5 Pervaporation measurement

The pervaporation apparatus, which was fabricated in-house, is shown in Scheme S1†. The effective area of the membrane in the permeation equipment was 3.14 cm^2. *n*-Butanol aqueous solutions with a composition of 1.0–6.0 wt.% were used as feed mixtures for the pervaporation experiments. The feed flow rate was controlled at 27 L h^{-1} by a peristaltic pump (BT300-1 J, Baoding Longer Precision Pump Co, Ltd., Hebei, China). The feed temperature was controlled by a thermostated water bath and was varied over the range of 30–80 °C. The feed-side temperature was measured by a sensor connected to a digital temperature gauge with an accuracy of ±0.1 °C (YF902C, Shenzhen Electronic Technology Co., Ltd., Shenzhen, China). The detection points were close to the module inlet (distance <8 cm). A vacuum pump (ZXZ-2, Linhai Tan Vacuum Equipment Co., Ltd., Linhai City, China) was connected to the permeating side to remove the vapor. The pressure in the permeation side was kept below 200 Pa and was monitored by a vacuum gauge with an accuracy of ±0.1 kPa. The permeated vapor was collected by a cold trap immersed in liquid nitrogen and then analyzed on a gas chromatograph (GC-2014, Shimadzu) with a thermal conductivity detector. Each membrane was analyzed three times by using the same pervaporation conditions. Parallel membranes were prepared in exactly the same manner. Fluxes were determined by measuring the weight of liquid collected in the cold traps over time (t) under steady-state conditions. The reported error represents the standard deviation of the average permeability obtained from independent measurements on three membrane samples. The permeation total flux (J) and separation factor (α), which represent the permeability and selectivity, respectively, were calculated according to the following equations:

$$J = \frac{Q}{At} \quad (1)$$

$$\alpha = \frac{(1 - Y_W) / Y_W}{(1 - X_W) / X_W} \quad (2)$$

where Q (g) is the total mass of the permeate collected in t hours; A (m^2) denotes the effective area of the membrane; and Y_W and X_W represent the water concentrations (wt.%) in the permeation and feed solutions, respectively.

The partial pressure differences (ΔP_i) and permeability coefficients (C_i) for component i were determined as follows:

$$\Delta P_i = P_{if} - P_{ip} \quad (3)$$

$$C_i = \frac{J_i l}{P_{if} - P_{ip}} \quad (4)$$

$$P_{if} = P_i^{sat} \gamma_i x_i \quad (5)$$

where P_{if} and P_{ip} are the partial pressure of component i over and under membrane, respectively; l is the thickness of the membrane; P_i^{sat}, γ_i and x_i are the saturation pressure, activity coefficient and mole fraction of component i over membrane. Activity coefficients of different feed concentrations were calculated by the Non-Random Two Liquid (NRTL) model[61] and saturation vapor pressure of butanol was calculated by the Antoine equation.

The overall separation factor (α) can be presented as the combination of the phase transition separation factor ($\alpha_{Phase.trans.}$), and membrane selectivity ($\alpha_{Membr.}$)[62], which were calculated as follows:

$$\alpha_{Phase.trans.} = \frac{(1 - X_W^{Vapor}) / X_W^{Vapor}}{(1 - X_W) / X_W} \quad (6)$$

$$\alpha_{Membr.} = \frac{(1 - Y_W) / Y_W}{(1 - X_W^{Vapor}) / X_W^{Vapor}} \quad (7)$$

$$\alpha = \alpha_{Phase.trans.} \alpha_{Membr.} \quad (8)$$

where X_W^{Vapor} represent the water concentrations (wt.%) in vapor phase over the membrane.

3. Results and discussion

3.1 Dispersion status of ZIF-8 in ethanol and PDMS solution

Nanoscale dispersion of ZIF-8 (Fig. S1 and Fig. S2†) leads to the formation of a homogeneous ZIF-8/PDMS solution. Therefore, it is necessary to study the dispersion of ZIF-8 nanoparticles in suspension before mixing it with PDMS solution. Fig. 1a shows that a stable ZIF-8 suspension was obtained before drying. To investigate the dispersion more intuitively, a small amount of suspension was applied onto a silicon wafer surface and was observed by SEM after drying. As shown in the SEM image, ZIF-8 nanoparticles exhibited a high degree of regularity and dispersion on the silicon wafer surface. After it was mixed with the PDMS solution, the ZIF-8 suspension-dispersed ZIF-8/PDMS solution were characterized in the same

manner that for ZIF-8 suspension (Fig. 1b). The suspension-dispersed ZIF-8/PDMS solution was stable, and the ZIF-8 nanoparticles were well dispersed in the ZIF-8/PDMS mixture (see SEM images in Fig. 1b). In contrast, the ZIF-8 powder suspension was unstable; precipitates settled at the bottom of the mixture (see Fig. S3a†). Therefore, serious particle agglomeration was observed by SEM. This instability is mainly due to the reaction of Zn–imidazole (Him) groups on the particle surface among themselves, forming strong covalent Zn–mim–Zn bonds between the particles during drying.[60] For this reason, the ZIF-8 powder was unstable in ZIF-8/PDMS solution, and it severely agglomerated in the ZIF-8/PDMS mixture (see SEM images in Fig. S3b†).

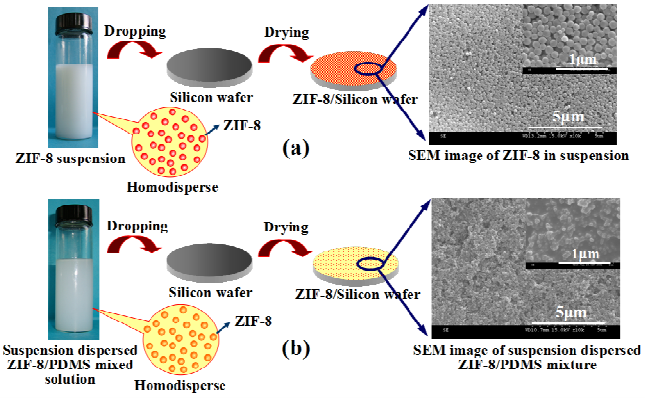

Fig. 1. Characterization process of the nanoparticle dispersion in (a) ZIF-8 suspension and (b) suspension-dispersed ZIF-8/PDMS mixed solution with the mass ratio of 1:1.

The dispersion of ZIF-8 particles in the PDMS matrix was also investigated by TEM. Fig. 2a and b shows TEM images of the suspension- and powder-dispersed ZIF-8/PDMS mixture precipitated in *n*-heptane. The suspension-dispersed ZIF-8/PDMS mixture had more uniform degree of dispersion of ZIF-8 nanoparticles. Meanwhile, there was strong interfacial interaction between ZIF-8 and PDMS (bottom right corner of Fig. 2a. This is because PDMS can act as a coating agent on the ZIF-8 surface, thereby reducing interphase voids in the mixture.[59] In contrast, dispersion of ZIF-8 in the powder-dispersed ZIF-8/PDMS mixture was poor, as evidenced by black agglomerates (Fig. 2b).

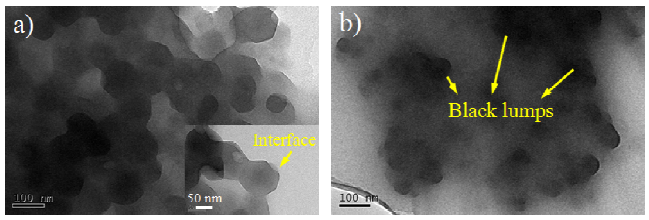

Fig. 2 TEM image of a) suspension-dispersed ZIF-8/PDMS mixture (bottom right corner, magnification TEM image of one segment) and b) powder-dispersed ZIF-8/PDMS mixture, ZIF-8/PDMS (1:1, w/w).

DLS is another effective method for determining particle dispersion. Through this method, we measured the apparent size distribution of ZIF-8 particle in the mixtures. Data from DLS of solutions may provide direct evidence of agglomeration.[63] Fig. 3 shows the narrow size distribution of ZIF-8 nanoparticles in the suspension; most of the particle sizes were close to 90 nm. This result indicates that the effects of centrifugation and solvents on the dispersion of ZIF-8 particles may be negligible. However, the particle size distribution of the ZIF-8 powder suspension became broad and even reached 600 nm. There was little change in particle size distribution in the suspension-dispersed ZIF-8/PDMS solution. Instead, the particle size distribution of the powder-dispersed ZIF-8/PDMS solution became broader and reached 1 μm because of ZIF-8 agglomeration. These results suggest mixing of the ZIF-8 suspension with the PDMS solution and the absence of particle agglomeration. The well-dispersed ZIF-8/PDMS solution was conducive to the formation of a homogeneous ZIF-8/PDMS nanohybrid membrane.

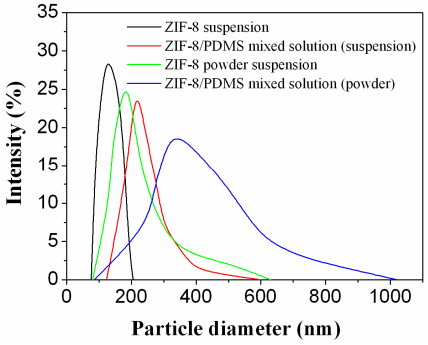

Fig. 3 Comparison of ZIF-8 particle size distribution under different conditions.

3.2 SEM, EDS, and XRD of suspension-dispersed ZIF-8/PDMS membrane

The surface morphologies of the PS supporting membrane and of the suspension-dispersed ZIF-8/PDMS membranes were characterized by SEM. A large number of pores on the PS supporting membrane may be clearly observed (Fig. 4a). In contrast, all of the surface pores were covered and no defects were found in a randomly selected area after multiple immersion in the suspension-dispersed ZIF-8/PDMS solution and further immersion in a concentrated PDMS pre-cross-linked solution (10 wt.%) (Fig. 4b). More importantly, ZIF-8 nanoparticles were dispersed uniformly in the PDMS layer and no obvious agglomeration was found. These observations are verified by the Zn signal from uniformly dispersed ZIF-8 in EDS mapping (Fig. 4c). For comparison, the powder-dispersed ZIF-8/PDMS membrane was prepared under the same conditions. ZIF-8 nanoparticles formed clusters in the PDMS layer of the powder-dispersed ZIF-8/PDMS membrane (see Fig. S4a†). EDS mapping (Fig. S4b†) also showed the poor distribution of Zn in the PDMS layer. XRD patterns confirm that ZIF-8 nanoparticles penetrated the PDMS layer and that they did not have altered crystallinity; diffraction peaks related to ZIF-8 were present in the patterns of the ZIF-8/PDMS membrane (Fig. 4d).

There are two main reasons for the high degree of dispersion of ZIF-8 nanoparticles in the suspension-dispersed ZIF-8/PDMS membrane. The ZIF-8 nanoparticles did not strongly interact with each other when they were not subjected to the standard drying procedure.[51,60,64–66] The ZIF-8 nanoparticle surface was coated with PDMS after dispersion of the ZIF-8 suspension in the PDMS solution. This primary coating prevented particles from touching each other and reduced interphase voids in the mixture.[35,59]

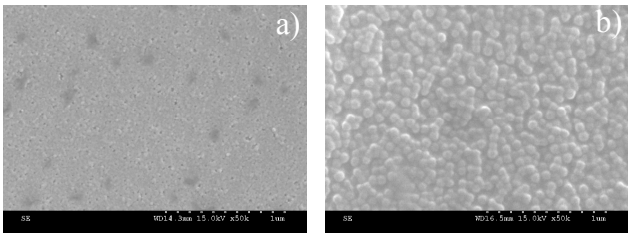

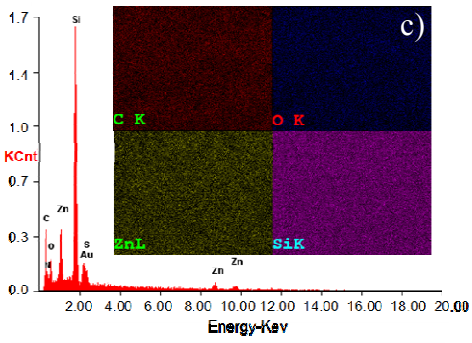

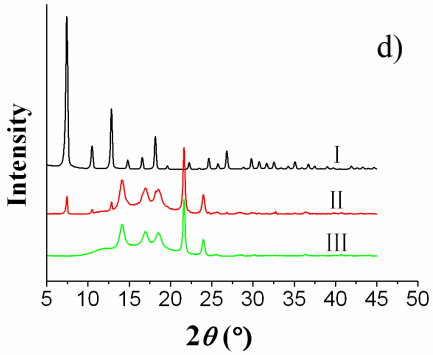

Fig. 4 Surface SEM images of a) PS supporting membrane and b) suspension-dispersed ZIF-8/PDMS nanohybrid membrane with the mass ratio of 1:1; c) Element analysis with EDS mapping of the suspension-dispersed ZIF-8/PDMS nanohybrid membrane surface; d) XRD patterns of (□) ZIF-8 nanoparticles, (□) suspension-dispersed ZIF-8/PDMS nanohybrid membrane and (□) pure PDMS membrane.

Comparisons using Fig. 5a and b show that the thickness of the selective layer of the suspension-dispersed ZIF-8/PDMS membrane was ~1.8 μm. However, it was difficult to obtain the exact thickness because the boundary between the selective layer and PS supporting membrane was not clear. In order to determine more accurately the thickness of the selective layer, changes in elemental composition through a membrane cross section were analyzed by EDS. As shown in Fig. 5c, the silicon content decreased while the sulfur content increased just after reaching 3.0 μm depth from the top layer. The concentrations of silicon and sulfur therefore show opposite trends. Since the PS supporting membrane does not contain silicon and PDMS does not contain sulfur, all of the silicon came from the PDMS selective layer and all of the sulfur came from the PS supporting membrane. As some of the silicon accumulated, some of the PDMS penetrated the PS membrane through its pores. It should be noted that the zinc signals remained low across the membrane cross section because of the relatively small amounts of ZIF-8 in PDMS.

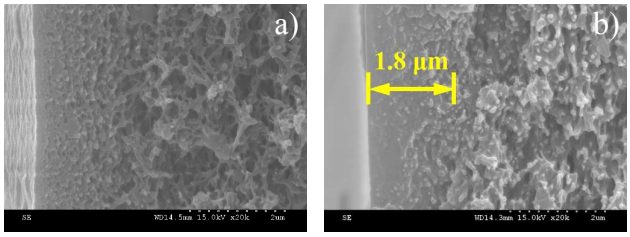

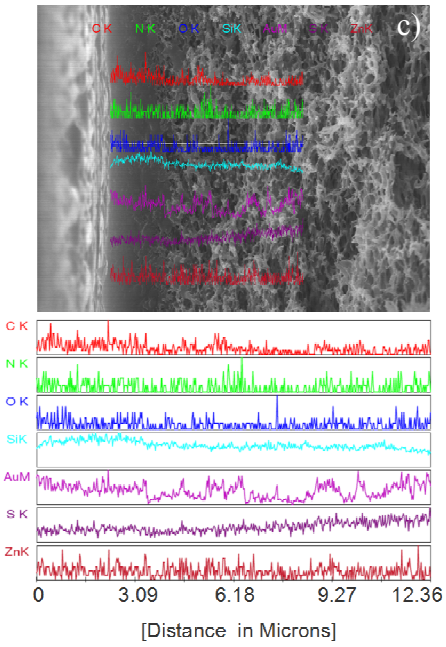

Fig. 5 Cross-sectional SEM images of the a) PS supporting membrane and b) suspension-dispersed ZIF-8/PDMS nanohybrid membrane with the mass ratio of 1:1; c) Cross-sectional EDS analyses of the suspension-dispersed ZIF-8/PDMS nanohybrid membrane.

3.3 Effects of immersion post-treatment, ZIF-8/PDMS mass ratio, and immersion layer on the membrane performance

Pervaporation is a very strict process that requires a nonporous membrane. Even minute defects cause a decline in selectivity.[67] It was found during the experiments that post-treatment by immersion of the nascent as-prepared ZIF-8/PDMS membrane in a concentrated PDMS pre-cross-linked solution (10 wt.%) had an important effect on the membrane pervaporation performance. When the nascent ZIF-8/PDMS membrane (mass ratio of 1:1) was removed from the suspension-dispersed ZIF-8/PDMS solution and then directly cross-linked at 80 °C without post-treatment, it was found to have poor separation factor but considerable flux (Fig. 6). Moreover, the separation factor of the ZIF-8/PDMS membrane without post-treatment (15.72; Fig. S5a†) showed little improvement over the pure PDMS composite membrane (13.13; Fig. S5c†) prepared under the same preparation conditions and even lower than that of pure PDMS composite membrane upon post-treatment (23.98; Fig. S5d†). Because immersion in a low concentration of suspension-dispersed ZIF-8/PDMS solution resulted in formation of an ultrathin selective layer (400 nm) on the PS supporting membrane surface (Fig. S5a†), some of the ZIF-8 nanoparticles were inevitably exposed on the membrane surface and were not embedded in the PDMS cross-linked layer. In this case, the ZIF-8 nanoparticles on the surface cannot participate in pervaporation. However, the ultrathin cross-linked layer can markedly increase the permeation flux because it has smaller transport resistance.[68,69] In contrast, the separation factor of the ZIF-8/PDMS nanohybrid membrane with post-treatment improved to 52.81. In addition, the ZIF-8/PDMS nanohybrid membrane subjected to further dip-coating exhibited a relatively high permeation flux (2800.54 g m^{-2} h^{-1}) because of the thin separation layer (1.8 μm thickness; Fig. S5b†). Meanwhile it should be noted that the separation factor of the pure PDMS composite membrane upon post-treatment only has a definite increase (23.98) due to the absence of ZIF-8 nanoparticles. Evidently, post-treatment by further immersion removed defects in the nascent ZIF-8/PDMS layers. It improved the separation factor significantly by coating all of the ZIF-8 nanoparticles. Therefore, all of the ZIF-8/PDMS nanohybrid membranes mentioned in the succeeding sections were subjected to post-treatment after multiple immersion in the suspension-dispersed ZIF-8/PDMS solution.

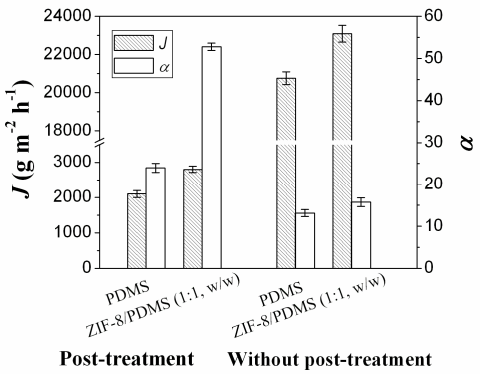

Fig. 6 Effect of post-treatment of dipping into concentrated PDMS pre-crosslinked solution (10wt.%) on the pervaporation performance; After two layers of dipping into suspension-dispersed ZIF-8/PDMS mixed solution (1wt.%, PDMS) or PDMS solution (1wt.%, PDMS) (shown in horizontal axis of Fig.6); Feed solution, 5.0 wt.% *n*-butanol aqueous solution at 80 °C; Error estimates were varied from 1.9 % to 4.6 % for the flux and from 1.7 % to 6.7 % for the separation factor.

The effect of ZIF-8/PDMS mass ratio in the suspension-dispersed ZIF-8/PDMS solution on the pervaporation performance is depicted in Fig. 7. Both permeation flux and separation factor of the suspension-dispersed ZIF-8/PDMS nanohybrid membranes in *n*-butanol recovery from 5.0 wt.% aqueous solution were much higher than those of pure PDMS composite membrane. Furthermore, there was a simultaneous increase in permeation flux and separation factor as the mass ratio of ZIF-8/PDMS increased. This anti-tradeoff phenomenon may be explained by the changes in membrane surface property and in ZIF-8 dispersity in the PDMS layer with the increase in mass ratio.[35,38,39,49] The nanohybrid membrane surface became more hydrophobic and the water contact angle increased from 105° (PS supporting membrane) to 124.5° at higher ZIF-8/PDMS mass ratio (2:1; Fig. S6†). Higher mass ratio also resulted in a smaller *n*-butanol contact angle, suggesting that doping with more ZIF-8 nanoparticles improved the affinity of the nanohybrid membrane to *n*-butanol. SEM images clearly show that ZIF-8 nanoparticles became more dispersed in the PDMS cross-linking layer as the mass ratio of ZIF-8/PDMS increased (0.5–1:1) (see Fig. S7†). In this case, ZIF-8 nanoparticles in PDMS can create more preferential pathways for *n*-butanol molecules through their ultrahigh adsorption selectivity.[70–73] Furthermore, the thin selective layer increases the permeation flux because of its lower diffusional resistance.[68,69] The low thickness of the top selective layer (~ 1.8 μm; Fig. 5b) led to high pervaporation performance of the membrane. The separation factor, however, decreased with further increase in ZIF-8/PDMS mass ratio (1.5:1). This anomaly may be attributed to agglomeration of ZIF-8 nanoparticles, as shown in Fig. S7†. For example, we observed that the ZIF-8 nanocrystals tended to aggregate into sub-micrometer particles at a ratio of 1.5:1 and higher. Therefore, the ZIF-8/PDMS solution with the optimum ZIF-8/PDMS mass ratio (1:1) was selected for subsequent experiments.

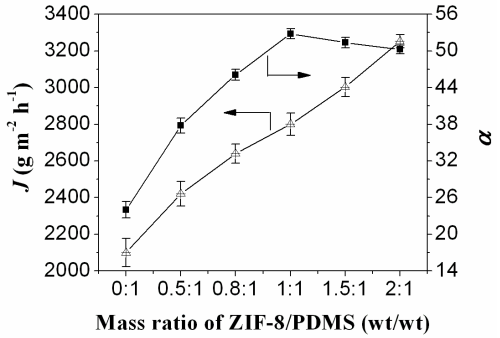

Fig. 7 Effect of the mass ratio of ZIF-8/PDMS in the suspension-dispersed mixed solution on the pervaporation performance; two layers of dipping into the ZIF-8/PDMS mixed solution (1 wt.%, PDMS), with post-treatment; feed solution, 5.0 wt.% *n*-butanol aqueous solution at 80 °C. Error estimates were varied from 1.1 % to 4.7 % for the flux and from 1.4 % to 5.6 % for the separation factor.

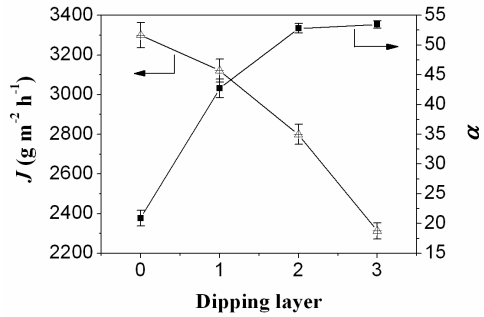

Fig. 8 Effect of dipping layers into the suspension-dispersed ZIF-8/PDMS (1:1, wt/wt) mixed solution on the pervaporation performance (1wt.%, PDMS), with post-treatment; feed solution, 5.0 wt.% *n*-butanol aqueous solution at 80°C. Error estimates were varied from 3.0 % to 4.3 % for the flux and from 1.1 % to 6.4 % for the separation factor.

Dipping layers have an important influence on the pervaporation performance. When the PS supporting membrane was post-treated by direct immersion in a pre-cross-linked PDMS solution at high concentration (10 wt.%) without immersion in the suspension-dispersed ZIF-8/PDMS solution, the membrane was found to exhibit the highest flux (3300 g m^{-2} h^{-1}) and the lowest separation factor (20.91) (Fig. 8). In this case, the separation function only depended on the cross-linked PDMS chains because of the absence of ZIF-8 nanoparticles in the selective layer, thereby leading to the lowest separation factor. The highest flux was due to the relatively thin separation layer obtained by direct immersion in 10 wt.% PDMS pre-cross-linked solution. The separation factor increased whereas the total flux decreased as the dipping cycles increased. This was expected because the ZIF-8/PDMS nanohybrid layer became more homogeneous and it became thicker with the increase in the number of dipping layers. We also observed that the separation factor barely increased as the number of dipping layers increased from two to three, whereas the total flux decreased markedly from 2800 to 2312.5 g m^{-2} h^{-1}. This indicates that once the separation layer became relatively uniform and dense, the selectivity became independent of any further increase in the number of dipping layers. Therefore, a compromise between pervaporation efficiency and number of dipping cycles was generally required. Two cycles, which were sufficient to achieve reasonable separation factor and suitable flux, was therefore used in subsequent experiments.

3.4 Effects of feed temperature and feed concentration on the pervaporation performance

Fig. 9a shows the influence of temperature on the pervaporation performance at a feed composition of 5 wt.% *n*-butanol aqueous solution. The permeation flux and separation factor increased simultaneously with increasing feed temperature, demonstrating the anti-tradeoff effect of the ZIF-8/PDMS nanohybrid membranes. The increase in permeation flux is due to the greater flexibility of polymer chains at higher temperature, which caused larger available free volumes of the PDMS cross-linking layer and larger gaps in the PDMS–ZIF-8 interface for diffusion of *n*-butanol and water.[74] Meanwhile, the increased difference in transmembrane vapor pressure of each component (Fig. 9b) caused by higher temperature enhanced the transport driving force.[17,75] The increase in separation factor may be explained by the increase in apparent activation energy of the permeation component. The calculated apparent activation energy of *n*-butanol (23.48 kJ mol^{-1}) was higher than that of water (12.36 kJ mol^{-1}), as determined according to the Arrhenius-type equation (Fig. S8(left)†)[74]

$$J_i = A_i \exp(-E_{P,i}/RT_b) \quad (9)$$

where J_i is the permeation flux of component i, A_i is the pre-exponential parameter of component i, $E_{P,i}$ is the apparent activation energy for the permeation of component i, R is the ideal gas constant, and T_b is the bulk liquid temperature. This difference indicates that *n*-butanol permeates preferentially at higher temperature. Moreover, the increase of total separation factor (α) could ascribe to much more rapid increase in phase transition separation factor ($\alpha_{Phase.trans.}$) in spite of the fact that membrane selectivity ($\alpha_{Membr.}$) decreases[76,77], as shown in in Fig. 9c. The increase in separation factor was lower at feed temperatures higher than at 50 °C because of the decreasing difference between the increment rates of *n*-butanol flux and water flux (Fig. S8 (right)†).

In addition, to estimate the real contribution of the membrane itself, the activation energy (E_m) could be calculated by extracting the enthalpies of evaporation from the apparent activation energy (E_p)[78], namely:

$$E_m = E_p - \Delta H_{evp} \quad (10)$$

Enthalpies of evaporation of *n*-butanol and water at 80°C are 46.95 and 41.5 kJ mol^{-1}, respectively. According to the calculated apparent activation energy of *n*-butanol and water (23.48 and 12.36 kJ/mol), The calculated E_m for *n*-butanol and water permeation in the membrane are -23.47 and -29.14kJ/mol, respectively. The negative E_m indicated that the permeability for both components decrease at higher temperature[62] (Fig. 9d). Moreover, because E_P consists of the activation energy for diffusion (which is always positive) and the heat of dissolution (which is often negative due to exothermic mixing process), a negative E_m indicates that the absolute value of the heat of dissolution is larger that that of the activation energy for diffusion. Therefore, for the *n*-butanol permselectivity of the membrane, the solubility selectivity caused by the strong affinity between *n*-butanol andthe organophilic membrane is the dominant step in pervaporation process.[34]

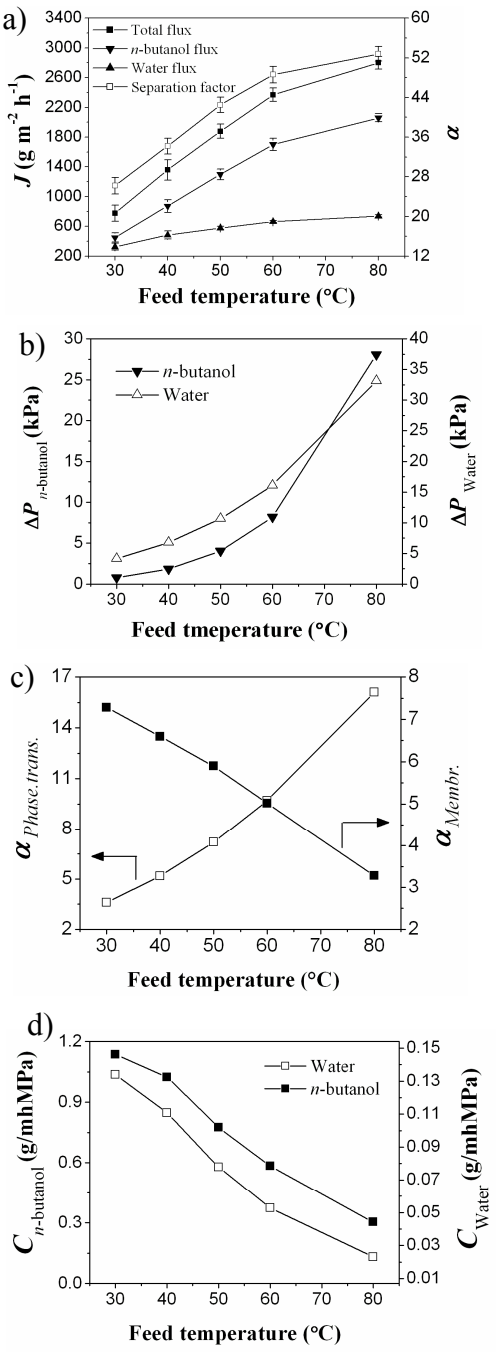

Fig. 9 Effect of feed temperature on a) pervaporation performance, b) partial pressure difference (driving force, *n*-butanol and water), c) permeability coefficient of *n*-butanol and water and d) contributions to total separation factor (membrane selectivity and phase transition separation factor) of the suspension-dispersed ZIF-8/PDMS nanohybrid membrane; two layers dipping into suspension-dispersed ZIF-8/PDMS (1:1, w/w) mixed solution feed solution (PDMS, 1 wt.%), with post-treatment; feed solution, 5 wt.% *n*-butanol aqueous solution. Error estimates were varied from 1.7% to 8.2% for the flux and from 2.7% to 8.9% for the separation factor.

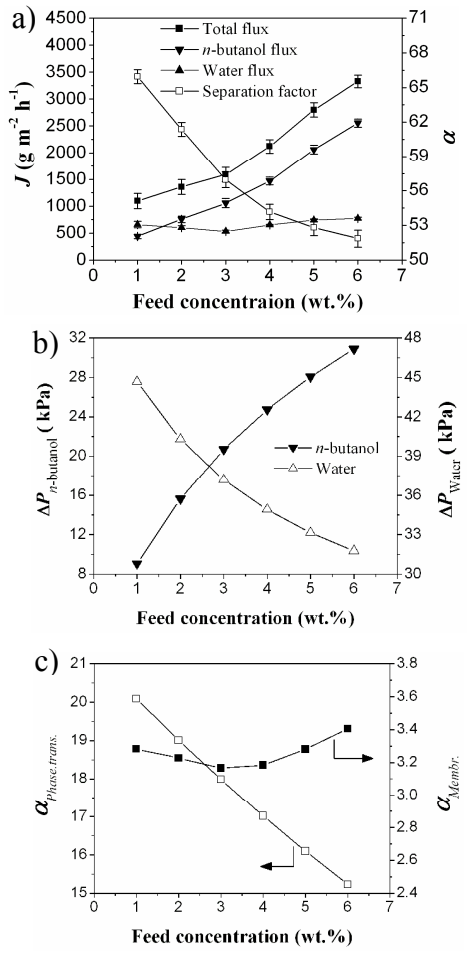

Fig. 10 Effect of feed concentration on the a) pervaporation performance, b) partial pressure difference (driving force, *n*-butanol and water) and c) contributions to total separation factor (membrane selectivity and phase transition separation factor) of the suspension-dispersed ZIF-8/PDMS nanohybrid membrane; two layers dipping into suspension-dispersed ZIF-8/PDMS (1:1, w/w) mixed solution feed solution (PDMS, 1 wt.%), with post-treatment; feed solution, *n*-butanol aqueous solution at 80 °C. Error estimates were varied from 2.0% to 7.5% for the flux and from 0.9% to 3.4% for the separation factor.

Fig. 10a shows the effect of *n*-butanol concentration in the feed solution on the pervaporation performance. The total flux increased with the increase in feed *n*-butanol concentration from 1 to 6 wt.%. Meanwhile, permeation fluxes of *n*-butanol and water increased with feed concentration, with the increase in *n*-butanol flux being more pronounced than that of the water flux. The reason for the increase in flux of *n*-butanol was its enhanced driving force due (Fig. 10b) to its increased sorption in the membrane at high *n*-butanol concentration.[34] Simultaneously, the increased sorption of *n*-butanol tended to increase the free volume and polymer chain flexibility, which facilitated water permeation through the membrane. Furthermore, the coupling effect originating from hydrogen bonding between water and *n*-butanol molecules resulted in an increase in water flux. It is worth noting that the total separation factor decreased with the increase of the feed concentration. This is mainly caused by the decrease of phase transition separation factor since the membrane selectivity varied within a very narrow range (Fig. 10c). Another reason is the denominator term in the formula for the separation factor (equation 2 in section 2.5) becomes large at high

n-butanol concentrations in the feed even if the *n*-butanol concentration in the permeate increases.[22]

3.5 Comparison of properties of the powder-dispersed ZIF-8/PDMS hybrid membrane and data in the literature

To illustrate clearly the superiority of the suspension-dispersed ZIF-8/PDMS membrane, a powder-dispersed ZIF-8/PDMS membrane prepared in the same manner as that for the ZIF-8/PDMS membrane was compared against it. The pervaporation performance of these two membranes in *n*-butanol recovery from aqueous solutions under the same operating conditions was evaluated, as shown in Fig. 11. The flux and separation factor of the suspension-dispersed ZIF-8/PDMS membrane were higher than those of the powder-dispersed ZIF-8/PDMS membrane. Moreover, they improved by 14.2% and 33.2%, respectively, over those of the powder-dispersed ZIF-8/PDMS membrane. The main reason for these differences is that the suspension-dispersed ZIF-8/PDMS solution was more conducive to formation of a homogeneous ZIF-8/PDMS nanohybrid membrane, as discussed in section 3.1. This maximizes the selectivity of ZIF-8 nanoparticles in adsorbing alcohol during pervaporation.[70] The calculated membrane selectivity of the suspension-dispersed ZIF-8/PDMS nanohybrid membrane is 3.3 larger than 2.5 (calculated by equation 7) of the powder-dispersed ZIF-8/PDMS membrane under the same operating conditions (5.0 wt.% *n*-butanol aqueous solution at 80 °C), which also demonstrates the former has a stronger selectivity to *n*-butanol.[77]

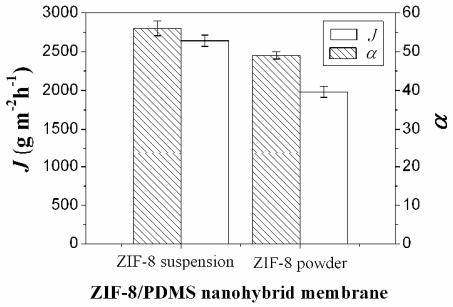

Fig. 11 Performance comparison of the suspension- and powder-dispersed ZIF-8/PDMS nanohybrid membrane; two layers of dipping into the ZIF-8/PDMS (1:1, w/w) mixed solution (PDMS, wt.%), with post-treatment; feed solution: 5.0 wt.% *n*-butanol aqueous solution at 80 °C. Error estimates were varied from 1.9 % to 4.8 % for the flux and from 2.7 % to 9.6 % for the separation factor.

Table S1† displays the pervaporation performance of various membranes in butanol/water mixtures. Most of the membranes were found to exhibit a typical tradeoff phenomenon. For example, the PVDF membrane exhibits high flux (4126 g m^{-2} h^{-1}) but poor separation factor (6.4) in the separation of 7.5 wt.% *n*-butanol/water solution at 50 °C.[74] In contrast, silicone-silicalite-1 membrane shows the highest separation factor (110) but much lower flux (70 g m^{-2} h^{-1}) at 78 °C in the separation of 1.0 wt.% *n*-butanol/water solution.[79] However, the suspension-dispersed ZIF-8/PDMS membrane in this study had a relatively high separation factor (42.5) and flux (1879.9 g m^{-2} h^{-1}) in the separation of 5.0 wt.% *n*-butanol/water solution at 50 °C. Furthermore, the suspension-dispersed ZIF-8/PDMS membrane exhibited higher overall performance compared with the other butanol permselective membranes, as shown in Fig. 12. Although the reported pervaporation data obtained from different conditions, at least, such comparison has demonstrated that the suspension-dispersed ZIF-8/PDMS nanohybrid membrane could be a potential candidate membrane material due to its comparable performance.

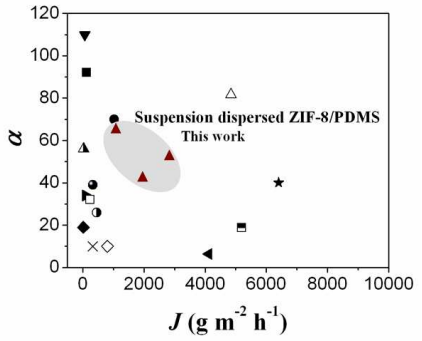

Fig. 12 Pervaporation performance in the recovery of butanol from aqueous solutions reported in previous studies and in our study.

4. Conclusions

An effective approach to overcome nanoparticle agglomeration during hybrid membrane formation was developed. This was done by directly dispersing a nascent ZIF-8 suspension in PDMS solution without further centrifuging and drying. SEM, TEM, and DLS analyses confirmed that the ZIF-8 suspension was mixed well with the PDMS solution and effectively diminished aggregation between nanoparticles. A homogeneous ZIF-8/PDMS nanohybrid membrane with a thin permselective layer (1.8 μm thickness) was obtained by repeated immersion of PS supporting membrane in a dilute ZIF-8/PDMS solution followed by removal of defects using a concentrated PDMS solution (post-treatment). The prepared suspension-dispersed ZIF-8/PDMS membrane had a high separation factor (52.81) and flux (2800.5 g m^{-2} h^{-1}) in the separation of 5.0 wt.% *n*-butanol/water solution at 80 °C. By comparing with the powder-dispersed ZIF-8/PDMS membrane, we found that the suspension-dispersed ZIF-8/PDMS membrane with uniform ZIF-8 dispersion showed much higher performance in butanol separation under the same conditions. As nanodispersion of inorganic nanoparticles in the polymer matrix is one of the most difficult and important issues in the preparation of high-performance hybrid membranes, this strategy may open a new way to design and prepare well-dispersed hybrid membranes and thus extend the use of these membranes to biofuel production and other uses.

Acknowledgements

This work was financially supported by the National High Technology Research and Development Program of China (No. 2012AA03A607), Program for New Century Excellent Talents in University, Ministry of Education, China (No. NCET-12-0604), Fok Ying Tung Education Foundation (No.131068) and Doctoral Fund of Innovation of Beijing University of Technology.

Notes and references

Center for Membrane Technology, College of Environmental and Energy Engineering, Beijing University of Technology, Beijing 100124, China. Fax: 86-10-6739 2393; *E-mail*: *zhanggj@bjut.edu.cn*

† Electronic Supplementary Information (ESI) available: [Schematic diagram of the pervaporation apparatus, SEM, EDS, contact angle and pervaporation measurement]. See DOI: 10.1039/b000000x/

1 M. Grayson. Biofuels, *Nature*, 2011, **474**, S1.
2 P. Fairly, *Nature*, 2011, **474**, S2–S5.
3 G. Stephanopoulos, *Science*, 2007, **315**, 801–804.
4 A. Demirbas, *Applied Energy*., 2011, **88**, 76–117.
5 N. Qureshi and T. C. Ezeji, *Biofuels*, *Bioprod*. *Bioref.,* 2008, **2**, 319–330.
6 N. Qureshi, B. C. Saha, B. Dien, R. E. Hector and M. A. Cotta, *Biomass Bioenergy*, 2010, **34**, 559–565.
7 H. J. Huang, S. Ramaswamy, U. W. Tschirner and B. V. Ramarao, *Sep*. *Purif*. *Technol*., 2008, **62**, 1–21.
8 L. M. Vane, *Biofuels, Bioprod. Bioref.,* 2008, **2**, 553–588.
9 L. Y. Jiang, Y. Wang, T. S. Chung, X. Y. Qiao and J. Y. Lai, *Prog*. *Polym*. *Sci*., 2009, **34**, 1135–1160.
10 C. Abels, F. Carstensen and M. Wessling, *J. Membr Sci.,* 2013, **444**, 285–317.
11 A. Oudshoorn, L. A. M. van der Wielen and A. J. J. Straathof, *Ind. Eng. Chem. Res*., 2009, **48**, 7325–7336.
12 M. García, M. T. Sanz and S. Beltrán, *J. Chem*. *Technol*. *Biotechnol*., 2009, **84**, 1873–1882.
13 F. Lipnizki, S. Hausmanns, G. Laufenberg, R. Field and B. Kunz, *Chem. Eng. Technol.*, 2000, **23**, 569–577.
14 L. M. Vane, *J. Chem*, *Technol*. *Biotechnol*.**,** 2005, **80**, 603–629.
15 Z. Dong, G. Liu, S. Liu, Z. Liu and W. Jin, *J. Membr Sci.,* 2014, **450**, 38–47.
16 J. Niemistö, W. Kujawski and R. L. Keiski, *J. Membr Sci.,* 2013, **434**, 55–64.
17 S. Y. Li, R. Srivastava and R. S. Parnas, *J. Membr Sci.,* 2010, **363**, 287–294.
18 G. P. Liu, W. Wei, H. Wu, X. L. Dong, M. Jiang and W. Q. Jin, *J. Membr. Sci.*, 2011, **373**, 121–129.
19 S. Li, F. Qin, P. Qin, M. N. Karim and T. Tan, *Green Chem*., 2013, **15**, 2180–2190.
20 D. M. Aguilar-Valencia, M. Á. Gómez-García and J. Fontalvo, *Ind. Eng. Chem. Res*., 2012, **51**, 9328–9334.
21 W. Van Hecke, P. Vandezande, S. Claes, S. Vangeel, H. Beckers, L. Diels and H. De Wever, *Bioresour. Technol*., 2012, **111**, 368–377.
22 X. Liu, Y. Li, Y. Liu, G. Zhu, J. Liu and W. Yang, *J. Membr Sci.,* 2011, **369**, 228–232.
23 G. Liu, W. Wei and W. Jin, *ACS Sustainable Chem. Eng*., 2014, **2**, 546−560
24 J. Caro, M. Noack and P. Kölsch, *Adsorption*, 2005, **11**, 215–227.
25 S. L. Wee, C. T. Tye and S. Bhatia, *Sep*. *Purif*. *Technol*., 2008, **63**, 500–516;
26 P. Peng, B. Shi and Y. Lan, *Sep*. *Sci*. *Technol*., 2011, **46**, 234–246.
27 D. Korelskiy, T. Leppäjärvi, H. Zhou, M. Grahn, J. Tanskanen and J. Hedlund, *J. Membr*. *Sci*., 2013, **427**, 381–389.
28 T. C. Bowen, R. D. Noble and J. L. Falconer, *J. Membr*. *Sci*., 2004, **245**, 1–33.
29 B. Zornoza, B. Seoane, J. M. Zamaro, C. Téllez and J. Coronas, *ChemPhysChem*., 2011, **12**, 2781–2785.
30 B. Zornoza, P. Gorgojo, C. Casado, C. Téllez and J. Coronas, *Desalin. Water. Treat.,* 2011, **27**, 42–47.
31 S. Claes, P. Vandezande, S. Mullens, K. De Sitter, R. Peeters and M. K. Van Bael, *J. Membr*. *Sci*., 2012, **389**, 265–271.
32 B. Zornoza, O. Esekhile, W. J. Koros, C. Téllez and J. Coronas, *Sep. Purif. Technol.,* 2011, **77**, 137–145.
33 B. Zornoza, C. Téllez. J. Coronas, J. Gascon and F. Kapteijn, *Microporous Mesoporous Mater.,* 2013, **166**, 67–78.
34 E. A. Fouad and X. Feng, *J. Membr Sci.,* 2009, **339**, 120–125.
35 S. N. Liu, G. P. Liu, X. H. Zhao and W. Q. Jin, *J. Membr. Sci.,* 2013, **446**, 181–188.
36 Y. Bai, L. Dong, C. Zhang, J. Gu, Y. Sun, L. Zhang, and H. Chen, *Sep. Sci. Technol.,* 2013**, 48**, 2531–2539.
37 H. Zhou, Y. Su, X. Chen, S. Yi, and Y. Wan, *Sep. Sci. Technol.,* 2010, **75**, 286–294.
38 X. L. Liu, Y. S. Li, G. Q. Zhu, Y. J. Ban, L. Y. Xu and W. S. Yang, *Angew. Chem. Int. Ed.*, 2011, **50**, 10636–10639.
39 Y. Li, L. H. Wee, J. Martens and I. Vankelecom, *J. Mater. Chem. A*., 2014, **2**, 10034–10040.
40 C. Sanchez, P. Belleville, M. Popalld and L. Nicole, *Chem. Soc. Rev.,* 2011, **40**, 696–753.
41 R. Nasir, H. Mukhtar, Z. Man and D. F. Mohshim, *Chem. Eng. Technol.*, 2013, **36**, 717–727.
42 G. M. Shi, T. Yang and T. S. Chung, *J. Membr. Sci.,* 2012, **415–416**, 577–586.
43 H. Vinh-Thang, and S. Kaliaguine, *Chem. Rev.***,** 2013, **113**, 4980–5028.
44 C. Liu, S. Kulprathipanja, A. M. W. Hillock, S. Husain and W. J. Koros, *Advanced Membrane Technology and Applications*., 2008, 787–819.
45 T. S. Chung, L. Y. Jiang, Y. Li and S. Kulprathipanja, *Prog. Polym. Sci.,* 2007, **32**, 483–507.
46 T. T. Moore, R. Mahajan, D. Q. Vu and W. J. Koros, *AIChE Journal*., 2004, **50**, 311–321.
47 T. T. Moore and W. J. Koros, *J. Mol. Struct.*, 2005, **739**, 87–98.
48 G. P. Liu, F. J. Xiangli, W. Wei, S. N. Liu and W. Q. Jin, *Chem. Eng. J.,* 2011, **174**, 495–503.
49 H. Fan, Q. Shi, H. Yan, S. Ji, J. Dong and G. Zhang, *Angew. Chem. Int. Ed.*, 2014, **53**, 5578–5582.
50 A. Nalaparaju, X. S. Zhao and J. W. Jiang, *Energy Environ. Sci*., 2011, **4**, 2107–2116.
51 T. Yang, Y. Xiao and T. S. Chung, *Energy Environ. Sci.*, 2011, **4**, 4171–4180.
52 H. R. Moon, D. W. Lim and M. P. Suh, *Chem. Soc. Rev.***,** 2013, **42**, 1807–1824.
53 M. E. Dose, *An Undergraduate Thesis*, **2013**, 5.
54 J. A. Thompson, K. W. Chapman, W. J. Koros, C. W. Jones and S. Nair, *Microporous Mesoporous Mater.*, 2012, **158**, 292–299.
55 J. Hilding, E. A. Grulke, Z. George Zhang and F. Lockwood, *J. Disper. Sci.Technol*., 2003, **24**, 1–41.
56 H. Zhou, R. Shi and W. Jin, *Sep. Sci. Technol.,* 2014, **127**, 61–69.
57 C. Liu, B. McCulloch, S. T. Wilson, A. I. Benin and M. E. Schott, *United States Patent.,* **2009**, Patent No.: US 7637983B1.
58 E. V. Perez, K. J. Balkus, Jr, J. P. Ferraris and I. H. Musselman, *J. Membr. Sci*., 2009, **328**, 165–173.
59 M. J. C. Ordoñez, K. J. Balkus, J. P. Ferraris and I. H. Musselman, *J. Membr. Sci.,* 2010, **361**, 28–37.
60 J. Cravillon, S. Münzer, S. J. Lohmeier, A. Feldhoff, K. Huber and M. Wiebcke, *Chem. Mater.,* 2009, **21**, 1410–1412.
61 J. Gmehling and U. Onken, Vapor-liquid Equilibrium Data Collection, Aqueous organic systems. *Chemistry data series*, Vol. **1**, Part **1**, D. Behrens, R. Eckermann, (Eds.) DECHEMA, Frankfurt, 1977.
62 A. V. Yakovlev, M. G. Shalygin, S. M. Matson, V. S. Khotimskiy and V. V. Teplyakow, *J. Membr. Sci.*, 2013, **434**, 99−105.

63 C. Courteille, C. Hollenstein, J. L. Dorier, P. Gay, W. Schwarzenbach, A. A. Howling, E. Bertran, G. Viera, R. Martins and A. Macarico, *J. Appl. Phys.,* 1996, **80**, 2069–2077.
64 M. Askari and T. S. Chung, *J. Membr. Sci.,* 2013, **444**, 173–183.
65 L. Diestel, X. L. Liu, Y. S. Li, W. S. Yang and J. Caro, *Microporous Mesoporous Mater.*, 2013, **189**, 210–215**.**
66 G. M. Shi, H. Chen, Y. C. Jean and T. S. Chung, *Polymer*, 2013, **54**, 774–783.
67 R. Wang, L. L. Shan, G. J. Zhang and S. L. Ji, *J. Membr. Sci.,* 2013, **432**, 33–41.
68 F. Xiangli, W. Wei, Y. Chen and W. Jin, N. Xu, *J. Membr. Sci.*, 2008, **311**, 23–33.
69 F. Xiangli, Y. Chen, W. Jin and N. Xu, *Ind. Eng. Chem. Res.,* 2007, **46**, 2224–2230.
70 K. Zhang, R. P. Lively, C. Zhang, R. R. Chance, W. J. Koros, D. S. Sholl and S. Nair, *J. Phys. Chem. Lett.*, 2013, **4**, 3618–3622.
71 K. Zhang, R. P. Lively, M. E. Dose, A. J. Brown, C. Zhang, J. Chung, S. Nair, W. J. Korosa and R. R. Chance, *Chem. Commun.,* 2013, **49**, 3245–3247.
72 P. Ksgens, M. Rose, I. Senkovska, H. Fre, A. Henschel, S. Siegle and S. Kaskel, *Microporous Mesoporous Mater.*, 2009, **120**, 325–330.
73 J. C. Saint Remi, T. Remy, V. V. Hunskerken, S. Perre, T. Duerinck, M. Maes, D. D. Vos, E. Gobechiya, C. E. A. Kirschhock, G. V. Baron and J. F. M. Denayer, *ChemSusChem*, 2011, **4**, 1074–1077.
74 K. Srinivasan, K. Palanivelu and A. N. Gopalakrishnan, *Chem. Eng. Sci.***,** 2007, **62**, 2905–2914.
75 Y. Huang, P. Zhang, J. Fu, Y. Zhou, X. B. Huang and X. Z. Tang, *J. Membr. Sci.*, 2009, **339**, 85–92.
76 R. W. Baker, J. G. Wijmans and Y. Huang, *J. Membr. Sci.*, 2010, **348**, 346−352.
77 I. L. Borisov, A. O. Malakhov, V. S. Khotimsky, E. G. Litvinova, E. Sh. Finkelshtein, N. V. Ushakov and V. V. Volkov, *J. Membr. Sci.*, 2014, **466**, 322−330.
78 X. Feng and R. Y. M. Huang, *J. Membr. Sci*. 1996, **118**, 127-131.
79 N. Qureshi, M. M. Meagher, R. W. Hutkins, *J. Membr. Sci.,*1999, **158**, 115–125.

Table of Content

Nanodisperse ZIF-8/PDMS Hybrid Membranes for Biobutanol Permselective Pervaporation

Hongwei Fan, Naixin Wang, Shulan Ji, Hao Yan, Guojun Zhang*

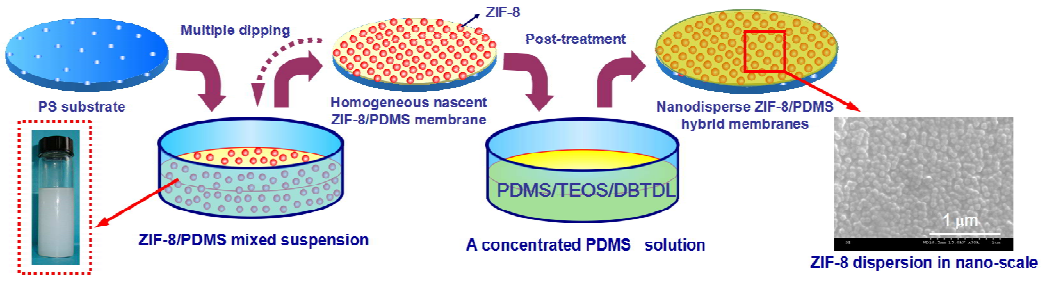

A homogeneous, nanodisperse ZIF-8/PDMS membrane was prepared by repeated immersion of a polysulfone supporting membrane in a dilute ZIF-8/PDMS suspension and subsequent removal of defects using a concentrated PDMS solution.